PROCEEDINGS OF THE ROYAL SOCIETY A

rspa.royalsocietypublishing.org

Statistical analysis and simulation of random shocks in stochastic Burgers equation

Heyrim Cho, Daniele Venturi and George E. Karniadakis

Division of Applied Mathematics, Brown University, Providence, RI 02912, USA

Research

Cite this article: Cho H, Venturi D, Karniadakis GE. 2014 Statistical analysis and simulation of random shocks in stochastic Burgers equation. *Proc. R. Soc. A* **470**: 20140080.
http://dx.doi.org/10.1098/rspa.2014.0080

Received: 30 January 2014
Accepted: 28 August 2014

Subject Areas:
applied mathematics, computational mathematics, statistical physics

Keywords:
hyperbolic conservation laws, Mori–Zwanzig formulation, discontinuous Galerkin methods

Author for correspondence:
G. E. Karniadakis
e-mail: george_karniadakis@brown.edu

We study the statistical properties of random shock waves in stochastic Burgers equation subject to random space–time perturbations and random initial conditions. By using the response–excitation probability density function (PDF) method and the Mori–Zwanzig (MZ) formulation of irreversible statistical mechanics, we derive exact reduced-order equations for the one-point and two-point PDFs of the solution field. In particular, we compute the statistical properties of random shock waves in the inviscid limit by using an adaptive (shock-capturing) discontinuous Galerkin method in both physical and probability spaces. We consider stochastic flows generated by high-dimensional random initial conditions and random additive forcing terms, yielding multiple interacting shock waves collapsing into clusters and settling down to a similarity state. We also address the question of how random shock waves in space and time manifest themselves in probability space. The proposed new mathematical framework can be applied to different conservation laws, potentially leading to new insights into high-dimensional stochastic dynamical systems and more efficient computational algorithms.

1. Introduction

In this paper, we study the statistical properties of the solution to the stochastic Burgers equation subject to random initial conditions and space–time additive random forcing terms. Although such a simple model cannot describe real fluid turbulence because of its explicit integrability and lack of chaotic character [1,2], it has been studied extensively as a useful benchmark to validate theoretical methods and computational algorithms. In particular, the so-called

Royal Society Publishing

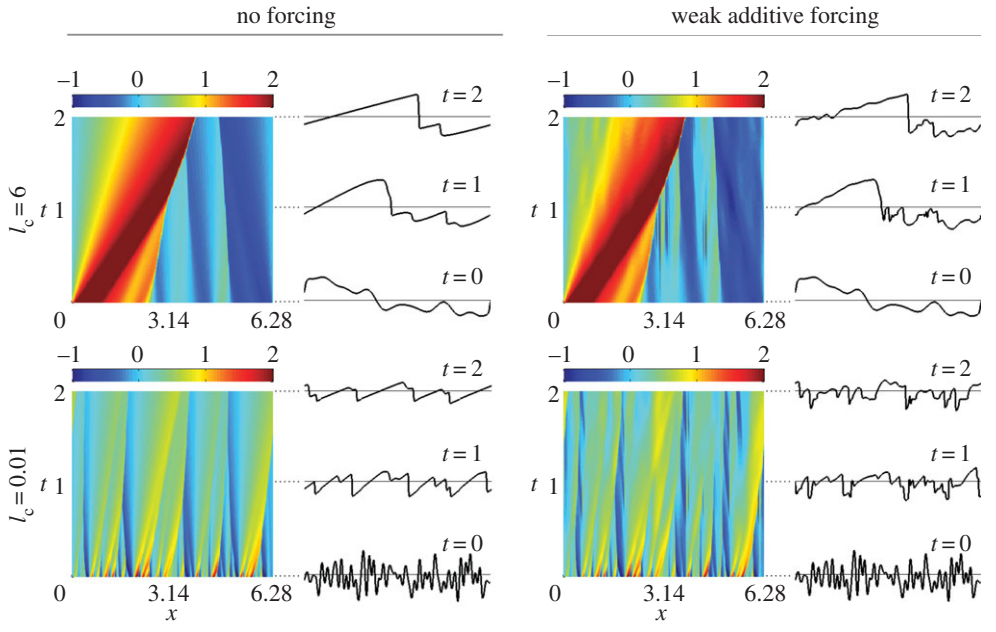

Figure 1. Sample solutions of the Burgers problem (2.1) in the inviscid limit $\nu \to 0$. Here, we consider two initial conditions with different correlation lengths randomly sampled from (3.6) and a realization of the random forcing term (3.5). It is seen that at $t = 2$ the velocity field already developed the triangular-shaped shock structure that is characteristic of the Burgers turbulence regime. Note that even weak additive forcing ($\sigma = 0.05$) can influence the solution, especially for rough initial conditions ($l_c = 0.01$). (Online version in colour.)

Burgers turbulence regime, i.e. the inviscid limit of the solution to the Burgers equation in the long-time integration, has been the subject of many investigations, e.g. [3–7]. It has been found that the statistical properties of the velocity field and the stochastic dynamics of the associated shock waves depend strongly on the probability distribution of both the initial data and the additive random forcing term. For example, Gaussian processes [4,6], white noise processes [7–12] and fractional Brownian motion perturbations in the initial condition [10,13,14] yield a completely different probabilistic structure of the velocity field. Similarly, additive random forcing terms can have a significant effect on the solution, e.g. they can generate anomalous shock displacement [15] and influence shock clustering [16–18] even at small amplitude. This is shown in figure 1, where we plot four realizations of the velocity field in the inviscid limit. Specifically, we consider solutions corresponding to two different initial conditions, randomly sampled from statistical ensembles with short and moderate correlation lengths. We also show the effects of weak additive forcing on the dynamics of the system.

To compute the statistical properties of the solution to stochastic Burgers problem, we need a representation of the functional relation between the state variables of the system and the random input processes. Well-known approaches are polynomial chaos [19–21], multi-element and sparse adaptive probabilistic collocation [22,23], high-dimensional model representations [24], stochastic biorthogonal expansions [25,26] and separated representations [27,28]. These techniques can provide considerable speed-up in computational time when compared to Monte Carlo (MC) or quasi-MC methods, and they are usually effective for the determination of the first few statistical moments of the solution. Here, we follow a different approach based on modelling, via deterministic equations, the probability density function (pdf) of the solution to the stochastic Burgers equation. The key idea stems from techniques of irreversible statistical mechanics, in particular, the Mori–Zwanzig (MZ) formalism [29–33], and it relies on deriving reduced-order kinetic equations for the stochastic velocity field in the limits of small viscosity and small perturbations. We combine this approach with the adaptive discontinuous Galerkin (DG)

method we have recently proposed in [34] to provide an efficient computational framework for the stochastic Burgers equation. The same framework can potentially be applied to more general system of stochastic conservation laws.

The paper is organized as follows. In §2, we derive the exact kinetic equation for the joint response-excitation PDF of the solution to the stochastic Burgers equation with parametrized random additive forcing. We also develop reduced-order kinetic equations for the single-point and the two-point PDF of the velocity field by using the MZ formalism. In particular, we determine a sequence of computable approximations based on Kubo–Van Kampen operator cumulant expansions. In §3, we perform stochastic simulations of the Burgers problem and compute the numerical solution to the MZ-PDF equations we derived in §2. To this end, we use the adaptive DG method described in appendix B. In particular, we study random flows induced by high-dimensional random initial conditions and random forcing terms, and discuss the statistical properties of the solution, including the shock development and clustering. Finally, the main findings and their implications are summarized in §4. We also include appendix A, where we briefly discuss shock waves in probability spaces.

2. Kinetic equations for Burgers turbulence

Let us consider the following prototype initial/boundary value problem for the Burgers equation

$$\left.\begin{aligned} &\frac{\partial u}{\partial t}+u\frac{\partial u}{\partial x}=\nu\frac{\partial^2 u}{\partial x^2}+\sigma f(x,t;\omega), \quad x\in[0,2\pi]\ \ t\geq 0,\\ &u(x,0;\omega)=u_0(x;\omega)\\ \text{and}\qquad &u(0,t;\omega)=u(2\pi,t;\omega), \end{aligned}\right\} \tag{2.1}$$

where the initial condition $u_0(x;\omega)$ and the forcing term $f(x,t;\omega)$ are square integrable random fields defined on a complete probability space. For each realization of $u_0(x;\omega)$ and $f(x,t;\omega)$, the solution $u(x,t;\omega)$ takes values in the space $L_2([0,2\pi],\mathbb{R})$ on which the operator $\partial^2/\partial x^2$ is endowed with periodic boundary conditions. The problem (2.1) is well-posed, since we can write $u\partial u/\partial x$ as $(\partial u^2/\partial x)/2$, which is locally Lipschitz from the Sobolev space[1] $\mathcal{W}^{1/4,2}$ into $\mathcal{W}^{-1,2}$, thus, allowing us to apply general local well-posedness theorems [35,36]. The regularity of the solution to equation (2.1) depends on the regularity of the random noise $f(x,t;\omega)$. In particular, if f is space–time white noise, then u has the regularity of Brownian motion, i.e. it is not differentiable in x. In this paper, we consider *smooth noise*, eventually yielding white noise as a result of a suitable limiting procedure. In particular, we represent $f(x,t;\omega)$ and $u_0(x;\omega)$ in terms of series expansions involving proper sets of random variables $\boldsymbol{\xi}(\omega)=\{\xi_1(\omega),\dots,\xi_m(\omega)\}$ and $\boldsymbol{\eta}(\omega)=\{\eta_1(\omega),\dots,\eta_l(\omega)\}$

$$u_0(x;\boldsymbol{\eta})=\sum_{k=1}^{l}\eta_k(\omega)\phi_k(x), \quad f(x,t;\boldsymbol{\xi})=\sum_{j=1}^{m}\xi_j(\omega)\Psi_j(x,t). \tag{2.2}$$

The existence and uniqueness of the solution to equation (2.1) for each realization of $u_0(x;\boldsymbol{\eta})$ and $f(x,t;\boldsymbol{\xi})$ allows us to consider the random field $u(x,t;\omega)$ as a deterministic function of $\boldsymbol{\xi}$ and $\boldsymbol{\eta}$, i.e. we have a *flow map* U such that

$$u(x,t;\omega)=U(x,t;\boldsymbol{\eta}(\omega),\boldsymbol{\xi}(\omega)). \tag{2.3}$$

Note that at initial time $U(x,0;\boldsymbol{\eta},\boldsymbol{\xi})=u_0(x;\boldsymbol{\eta})$. The joint PDF of the solution to equation (2.1) and the random vector $\boldsymbol{\xi}(\omega)$ admits the following representation (see, e.g. [37–39]):

$$p(x,t;a,\boldsymbol{b})=\int_{-\infty}^{\infty}\cdots\int_{-\infty}^{\infty}\delta(a-U(x,t;\boldsymbol{A}_0,\boldsymbol{B}))\delta(\boldsymbol{b}-\boldsymbol{B})q(\boldsymbol{A}_0,\boldsymbol{B})\,\mathrm{d}\boldsymbol{A}_0\,\mathrm{d}\boldsymbol{B}, \tag{2.4}$$

[1]The Sobolev space is defined as $\mathcal{W}^{k,p}\overset{\text{def}}{=}\{u\in L^p : D^\alpha u\in L^p,\ \forall\,|\alpha|\leq k\}$.

where $a \in \mathbb{R}$, $\boldsymbol{b} \in \mathbb{R}^m$, $\boldsymbol{A}_0 \in \mathbb{R}^l$, $\boldsymbol{B} \in \mathbb{R}^m$, $q(\boldsymbol{A}_0, \boldsymbol{B})$ denotes the (possibly compactly supported) joint PDF of the random vectors $\boldsymbol{\eta}$ and $\boldsymbol{\xi}$, and $\delta(\boldsymbol{b} - \boldsymbol{B})$ is a multi-dimensional Dirac delta function, i.e.

$$\delta(\boldsymbol{b} - \boldsymbol{B}) \overset{\text{def}}{=} \prod_{k=1}^{m} \delta(b_k - B_k).$$

The one-point one-time PDF of the solution to equation (2.1) is obtained by integrating (2.4) with respect to $\boldsymbol{b} = \{b_1, \ldots, b_m\}$

$$p_u(x,t;a) = \int_{-\infty}^{\infty} \cdots \int_{-\infty}^{\infty} p(x,t;a,\boldsymbol{b})\, \mathrm{d}\boldsymbol{b}. \tag{2.5}$$

Differentiating (2.4) with respect to x and t and using suitable identities involving the Dirac delta function yields the following exact joint response-excitation PDF equation[2]:

$$\frac{\partial p(t)}{\partial t} + \int_{-\infty}^{a} \frac{\partial p(t)}{\partial x}\, \mathrm{d}a' + a\frac{\partial p(t)}{\partial x} = -\sigma f(x,t;\boldsymbol{b})\frac{\partial p(t)}{\partial a} - \nu \frac{\partial}{\partial a}\left\langle \frac{\partial^2 u}{\partial x^2}\delta(a - u(x,t))\right\rangle, \tag{2.6}$$

where we used the shorthand notation $p(t) \equiv p(x,t;a,\boldsymbol{b})$. The last term on the right-hand side is defined as

$$\left\langle \frac{\partial^2 u}{\partial x^2}\delta(a - u(x,t))\right\rangle \overset{\text{def}}{=} \int_{-\infty}^{\infty} \cdots \int_{-\infty}^{\infty} \frac{\partial^2 U}{\partial x^2}\delta(a - U(x,t;\boldsymbol{A}_0,\boldsymbol{B})) \times \delta(\boldsymbol{b} - \boldsymbol{B}) q(\boldsymbol{A}_0,\boldsymbol{B})\, \mathrm{d}\boldsymbol{A}_0\, \mathrm{d}\boldsymbol{B}, \tag{2.7}$$

and it represents an *unclosed* term that has to be treated using *closure models* having additional assumptions [40,41]. For example, we can introduce a conditional average $\langle u_{xx}|u\rangle$[3] and rewrite (2.6) as

$$\frac{\partial p(t)}{\partial t} + \int_{-\infty}^{a} \frac{\partial p(t)}{\partial x}\, \mathrm{d}a' + a\frac{\partial p(t)}{\partial x} = -\sigma f(x,t;\boldsymbol{b})\frac{\partial p(t)}{\partial a} - \nu \frac{\partial}{\partial a}\left[\left\langle \frac{\partial^2 u}{\partial x^2}\,\middle|\, u\right\rangle p_u(t)\right]. \tag{2.8}$$

An interesting question is what happens to the solution to the PDF equations (2.6) or (2.8) in the limit of zero viscosity $\nu \to 0$. In this case, equation (2.1) becomes a hyperbolic conservation law that can generate shock discontinuities at random space–time locations (see figure 1 for a few solution samples). There has been extensive theoretical investigation of the inviscid limit to the solution to the viscous Burgers equation (e.g. [7,13,42]). From the PDF standpoint, the inviscid limit influences the conditional average in equation (2.8). In particular, it contributes sharply to the PDF dynamics nearby the space–time locations where random shocks develop. This is sometimes referred to as dissipative anomalies [41]. As we shall see in §3, the numerical dissipation associated with finite resolution in numerical simulations of equations (2.1) and (2.8) dominates the regularizing diffusion terms for $\nu \to 0$. Therefore, from a numerical standpoint, we could set $\nu = 0$ in equations (2.1) and (2.8) and study the inviscid limit of the Burgers equation in the sense of *vanishing numerical viscosity* for increasing levels of resolution.

[2]Note that differentiating (2.6) with respect to a allows us to remove the integral term and it yields a second-order linear PDE.

[3]The conditional average is explicitly defined as

$$\langle u_{xx}|u\rangle \overset{\text{def}}{=} \int_{-\infty}^{\infty} \cdots \int_{-\infty}^{\infty} U_{xx}\delta(a - U(x,t;\boldsymbol{A}_0,\boldsymbol{B}))\delta(\boldsymbol{b} - \boldsymbol{B})\tilde{q}(\boldsymbol{A}_0,\boldsymbol{B}|u = a)\, \mathrm{d}\boldsymbol{A}_0\, \mathrm{d}\boldsymbol{B}.$$

(a) Reduced-order PDF equations: MZ approach

Let us set $\nu = 0$ in the PDF equation (2.8) and rewrite it in a Liouville-type form as

$$\frac{\partial p(t)}{\partial t} = [\mathcal{L}_0 + \sigma \mathcal{L}_1(t)]p(t), \tag{2.9}$$

where

$$\mathcal{L}_0 \stackrel{\text{def}}{=} -\int_{-\infty}^{a} \mathrm{d}a' \frac{\partial}{\partial x} - a\frac{\partial}{\partial x} \quad \text{and} \quad \mathcal{L}_1(t) \stackrel{\text{def}}{=} -f(x,t;\boldsymbol{b})\frac{\partial}{\partial a}. \tag{2.10}$$

Since $\mathcal{L}_0$ is a time-independent linear operator, it is convenient to integrate out exactly the dynamics associated with it first, so as to circumscribe the approximation problem to $\mathcal{L}_1(t)$. This can be carried out by means of a preliminary time-dependent transformation

$$w(t) = \mathrm{e}^{-t\mathcal{L}_0}p(t), \tag{2.11}$$

which is known as *interaction picture* in quantum mechanics. Substituting (2.11) into equation (2.9) yields

$$\frac{\mathrm{d}w(t)}{\mathrm{d}t} = \sigma \mathcal{N}(t)w(t), \quad \mathcal{N}(t) \stackrel{\text{def}}{=} \mathrm{e}^{-t\mathcal{L}_0}\mathcal{L}_1(t)\,\mathrm{e}^{t\mathcal{L}_0}. \tag{2.12}$$

Note that $\mathcal{L}_0$ depends only on the phase variable a, representing the velocity field, but not on the phase variables $\boldsymbol{b}$ associated with the random forcing term. This implies that the PDF of $u(x,t;\omega)$ can be, in principle, obtained by inverting equation (2.11) and then integrating it with respect to $\boldsymbol{b}$. This operation can be conveniently represented in terms of an orthogonal projection operator

$$\mathcal{P}p(t) \stackrel{\text{def}}{=} q(\boldsymbol{b}) \int_{-\infty}^{\infty} \cdots \int_{-\infty}^{\infty} p(t)\,\mathrm{d}\boldsymbol{b}, \tag{2.13}$$

where $q(\boldsymbol{b})$ denotes the joint PDF of the random vector $\boldsymbol{\xi}$ appearing in the forcing term. Note that $\mathcal{P}^2 = \mathcal{P}$ and that $\mathcal{P}\mathcal{L}_0 = \mathcal{L}_0\mathcal{P}$, i.e. $\mathcal{P}$ commutes with $\mathcal{L}_0$. In addition, integration of equation (2.13) with respect to $\boldsymbol{b}$ yields $p_u(t)$, that is, the one-point one-time PDF of the velocity field that solves equation (2.1) in the inviscid limit. If we apply $\mathcal{P}$ to both sides of equation (2.11), differentiate it with respect to t, and integrate with respect to $\boldsymbol{b}$, we obtain

$$\frac{\partial p_u(t)}{\partial t} = \mathcal{L}_0 p_u(t) + \mathrm{e}^{t\mathcal{L}_0} \int_{-\infty}^{\infty} \cdots \int_{-\infty}^{\infty} \frac{\partial \mathcal{P}w(t)}{\partial t}\,\mathrm{d}\boldsymbol{b}. \tag{2.14}$$

The next step is to determine the law for $\partial \mathcal{P}w(t)/\partial t$. This can be done in a formally exact way by using the MZ formalism, in particular, the convolutionless form [29,31,32]. This yields

$$\frac{\partial \mathcal{P}w(t)}{\partial t} = \hat{\mathcal{K}}(t)\mathcal{P}w(t) + \hat{\mathcal{H}}(t)\mathcal{Q}w(0), \tag{2.15}$$

where $\mathcal{Q} \stackrel{\text{def}}{=} \mathcal{I} - \mathcal{P}$,

$$\hat{\mathcal{K}}(t) \stackrel{\text{def}}{=} \sigma \mathcal{P}\mathcal{N}(t)[\mathcal{I} - \sigma\hat{\Sigma}(t)]^{-1}, \tag{2.16}$$

$$\hat{\mathcal{H}}(t) \stackrel{\text{def}}{=} \sigma \mathcal{P}\mathcal{N}(t)[\mathcal{I} - \sigma\hat{\Sigma}(t)]^{-1}\hat{\mathcal{G}}(t,0) \tag{2.17}$$

$$\hat{\Sigma}(t) \stackrel{\text{def}}{=} \int_0^t \hat{\mathcal{G}}(t,s)\mathcal{Q}\mathcal{N}(s)\mathcal{P}\hat{\mathcal{Z}}(t,s)\,\mathrm{d}s, \tag{2.18}$$

and

$$\hat{\mathcal{G}}(t,s) \stackrel{\text{def}}{=} \overleftarrow{\mathcal{T}} \exp\left[\sigma \int_s^t \mathcal{Q}\mathcal{N}(\tau)\,\mathrm{d}\tau\right], \quad \hat{\mathcal{Z}}(t,s) \stackrel{\text{def}}{=} \overrightarrow{\mathcal{T}} \exp\left[-\sigma \int_s^t \mathcal{N}(\tau)\,\mathrm{d}\tau\right]. \tag{2.19}$$

In equation (2.19), $\overleftarrow{\mathcal{T}}$ and $\overrightarrow{\mathcal{T}}$ denote, respectively, the chronological and the anti-chronological time-ordering operators. If the joint PDF $p(0) = w(0)$ is separable, i.e. if the initial condition $u(x,0;\boldsymbol{\eta})$ is independent of the random excitation vector $\boldsymbol{\xi}$, then $w(0)$ is in the range of $\mathcal{P}$ and we have $\mathcal{Q}w(0) = 0$ in equation (2.15). In the following, we will consider such case.

So far everything that has been said is exact and it has led us to equations (2.14) and (2.15), which are linear and of infinite order in the phase variable a. We now introduce approximations. To this end, we expand the right-hand side of equation (2.15) in formal power series in the coupling parameter σ (see [29] for details). This yields

$$\frac{\partial \mathcal{P}w(t)}{\partial t} = \left(\sigma \mathcal{N}(t) + \sigma^2 \int_0^t [\mathcal{P}\mathcal{N}(t)\mathcal{N}(s) - \mathcal{P}\mathcal{N}(t)\mathcal{P}\mathcal{N}(s)]\,\mathrm{d}s + \cdots\right)\mathcal{P}w(t). \tag{2.20}$$

Substituting (2.20) into equation (2.14) gives the reduced order kinetic equation

$$\frac{\partial p_u(t)}{\partial t} = \mathcal{L}_0 p_u(t) + \mathrm{e}^{t\mathcal{L}_0}\left(\sigma \langle \mathcal{N}(t)\rangle_K + \sigma^2 \int_0^t \langle \mathcal{N}(t)\mathcal{N}(s)\rangle_K\,\mathrm{d}s + \cdots\right)\mathrm{e}^{-t\mathcal{L}_0} p_u(t), \tag{2.21}$$

where $\langle \mathcal{N}(t_1)\cdots\mathcal{N}(t_n)\rangle_K$ are Kubo–Van Kampen operator cumulants [29,43,44] relative to the joint PDF of the random vector $\boldsymbol{\xi}$. For instance, the first two cumulants are

$$\langle \mathcal{N}(t)\rangle_K = \int_{-\infty}^{\infty}\cdots\int_{-\infty}^{\infty} \mathcal{N}(t) q(\boldsymbol{b})\,\mathrm{d}\boldsymbol{b} \tag{2.22}$$

and

$$\langle \mathcal{N}(t)\mathcal{N}(s)\rangle_K = \int_{-\infty}^{\infty}\cdots\int_{-\infty}^{\infty} [\mathcal{N}(t)\mathcal{N}(s)q(\boldsymbol{b}) - \mathcal{N}(t)q(\boldsymbol{b})\mathcal{N}(s)q(\boldsymbol{b})]\,\mathrm{d}\boldsymbol{b}, \tag{2.23}$$

each one being a linear operator in the phase variables a and x. The nth order operator cumulant $\langle \mathcal{N}(t_1)\cdots\mathcal{N}(t_n)\rangle_K$ can be calculated by using diagrammatic methods [43]. The reduced-order kinetic equation (2.21) is linear, formally exact, but it involves derivatives of infinite-order in both variables x and a. Such derivatives come from the operator cumulants as well as from the exponential operators appearing in equations (2.12) and (2.21). In a finite-dimensional setting, these quantities can be computed by using efficient numerical algorithms, e.g. based on scaling-squaring techniques, Padé approximants, or Krylov subspace projection methods [45–48]. Any finite-order truncation of the series within the brackets in equation (2.21) yields an approximation whose accuracy depends on the magnitude of σ, the integration time t, as well as on the decay rate of the Kubo–Van Kampen operator cumulants $\langle \mathcal{N}(t_1)\cdots\mathcal{N}(t_n)\rangle_K$. The latter depends on the properties of the random forcing. For example, in Langevin systems forced with Gaussian white noise it can be shown that the approximation obtained by retaining only the first two operator cumulants is exact for arbitrary σ (see [29]).

We remark that the kinetic equation (2.21) can also be derived by using the asymptotic perturbation theory of semigroups [49,50]. The simplest way to do so is to consider the formal (implicit) solution to equation (2.9)

$$p(t) = \mathrm{e}^{t\mathcal{L}_0} p(0) + \sigma \int_0^t \mathrm{e}^{(t-s)\mathcal{L}_0}\mathcal{L}_1(s) p(s)\,\mathrm{d}s, \tag{2.24}$$

and generate a sequence of approximations by recursive substitution, starting from $p(0)$. This yields

$$\begin{aligned} p(t) = \Bigg[&\mathrm{e}^{\mathcal{L}_0(t)} + \sigma \int_0^t \mathrm{e}^{(t-s)\mathcal{L}_0}\mathcal{L}_1(s)\,\mathrm{e}^{s\mathcal{L}_0}\,\mathrm{d}s \\ &+\sigma^2 \int_0^t\int_0^s \mathrm{e}^{\mathcal{L}_0(t-s)}\mathcal{L}_1(s)\,\mathrm{e}^{(s-z)\mathcal{L}_0}\mathcal{L}_1(z)\,\mathrm{e}^{z\mathcal{L}_0}\,\mathrm{d}z\,\mathrm{d}s\Bigg] p(0) + O(\sigma^3). \end{aligned} \tag{2.25}$$

Assuming that $p(0)$ is separable as $p(0) = p_u(0)q(\boldsymbol{b})$, integrating equation (2.25) with respect to $\boldsymbol{b}$ yields the second-order approximation to the formal analytical solution to equation (2.21), i.e.

$$\begin{aligned} p_u(t) = \Bigg[&\mathrm{e}^{\mathcal{L}_0(t)} + \sigma \int_0^t \mathrm{e}^{(t-s)\mathcal{L}_0}\langle\mathcal{L}_1(s)\rangle_{\boldsymbol{b}}\,\mathrm{e}^{s\mathcal{L}_0}\,\mathrm{d}s \\ &+\sigma^2 \int_0^t\int_0^s \mathrm{e}^{\mathcal{L}_0(t-s)}\langle\mathcal{L}_1(s)\,\mathrm{e}^{(s-z)\mathcal{L}_0}\mathcal{L}_1(z)\rangle_{\boldsymbol{b}}\,\mathrm{e}^{z\mathcal{L}_0}\,\mathrm{d}z\,\mathrm{d}s\Bigg] p_u(0) + O(\sigma^3), \end{aligned} \tag{2.26}$$

where

$$\langle\cdot\rangle_{\boldsymbol{b}} \overset{\text{def}}{=} \int_{-\infty}^{\infty}\cdots\int_{-\infty}^{\infty}(\cdot)q(\boldsymbol{b})\,\mathrm{d}\boldsymbol{b}. \tag{2.27}$$

An interesting subcase of equations (2.14) and (2.26) is obtained by assuming that the random forcing does not depend on x. This yields the simplified kinetic equation

$$\frac{\partial p_u(t)}{\partial t} = \mathcal{L}_0 p_u(t) + \sigma\langle f(t;\boldsymbol{b})\rangle_{\boldsymbol{b}}\frac{\partial p_u(t)}{\partial a} + \sigma^2\int_0^t\left(\mathrm{e}^{(t-s)\mathcal{L}_0}C(t,s)\frac{\partial^2 p_u(s)}{\partial a^2}\right.$$
$$\left. - (t-s)\,\mathrm{e}^{(t-s)\mathcal{L}_0}\langle f(t;\boldsymbol{b})f(s;\boldsymbol{b})\rangle_{\boldsymbol{b}}\frac{\partial^2 p_u(s)}{\partial x\partial a}\right)\mathrm{d}s + O(\sigma^3), \tag{2.28}$$

where $C(t,s)$ is the temporal covariance of $f(t;\boldsymbol{\xi})$. Equation (2.28) is obtained by differentiating equation (2.26) with respect to time and noting that

$$\begin{aligned}\mathcal{L}_1(t)\,\mathrm{e}^{(s-u)\mathcal{L}_0} &= \sum_{n=0}^{\infty}\frac{1}{n!}\mathcal{L}_1(t)\mathcal{L}_0^n(s-u)^n\\ &= \sum_{n=0}^{\infty}\frac{1}{n!}\left(\mathcal{L}_0^n\mathcal{L}_1(t) - n\mathcal{L}_0^{n-1}f(t;\boldsymbol{b})\frac{\partial}{\partial x}\right)(s-u)^n\\ &= \mathrm{e}^{(s-u)\mathcal{L}_0}\mathcal{L}_1(t) - (s-u)\,\mathrm{e}^{(s-u)\mathcal{L}_0}f(t;\boldsymbol{b})\frac{\partial}{\partial x}.\end{aligned}$$

(b) Kinetic equations for the two-point PDF

Let us consider the two-point joint response-excitation PDF, i.e. the joint PDF of $u(x_1,t;\omega)$, $u(x_2,t;\omega)$ and $\boldsymbol{\xi}$,

$$p_2(x_1,x_2,t;a_1,a_2,\boldsymbol{b}) = \int_{-\infty}^{\infty}\cdots\int_{-\infty}^{\infty}\prod_{i=1}^{2}\delta(a_i - U(x_i,t;\boldsymbol{A}_0,\boldsymbol{B}))$$
$$\times\,\delta(\boldsymbol{b}-\boldsymbol{B})q(\boldsymbol{A}_0,\boldsymbol{B})\,\mathrm{d}\boldsymbol{A}_0\,\mathrm{d}\boldsymbol{B}. \tag{2.29}$$

Such PDF satisfies the obvious limiting condition

$$\lim_{x_1\to x_2} p_2(x_1,x_2,t;a_1,a_2,\boldsymbol{b}) = \delta(a_1-a_2)p(x_1,t;a_1,\boldsymbol{b}), \tag{2.30}$$

where $p(x_1,t;a_1,\boldsymbol{b})$ is the one-point PDF (2.4). It can be shown (see, e.g. [37,38]) that in the inviscid limit $\nu\to 0$, the PDF (2.29) satisfies the exact kinetic equation

$$\frac{\partial p_2(t)}{\partial t} = [\mathcal{H}_0 + \sigma\mathcal{H}_1(t)]p_2(t), \tag{2.31}$$

where

$$\mathcal{H}_0 \overset{\text{def}}{=} -\sum_{i=1}^{2}\left(\int_{-\infty}^{a_i}\mathrm{d}a_i'\frac{\partial}{\partial x_i} + a_i\frac{\partial}{\partial x_i}\right),\quad \mathcal{H}_1(t) \overset{\text{def}}{=} -\sum_{i=1}^{2}f(x_i,t;\boldsymbol{b})\frac{\partial}{\partial a_i}. \tag{2.32}$$

By following the same mathematical steps that led us to equation (2.21), we obtain the following reduced-order kinetic equation for the two-point PDF of the solution field[4]

$$\frac{\partial p_{uu'}(t)}{\partial t} \simeq \mathcal{H}_0 p_{uu'}(t) + \mathrm{e}^{t\mathcal{H}_0}\left(\sigma\langle\mathcal{G}(t)\rangle_K + \sigma^2\int_0^t\langle\mathcal{G}(t)\mathcal{G}(s)\rangle_K\,\mathrm{d}s + \cdots\right)\mathrm{e}^{-t\mathcal{H}_0}p_{uu'}(t), \tag{2.33}$$

where

$$\mathcal{G}(t) \overset{\text{def}}{=} \mathrm{e}^{-t\mathcal{H}_0}\mathcal{H}_1(t)\,\mathrm{e}^{t\mathcal{H}_0}. \tag{2.34}$$

[4]Here, we use the shorthand notation $p_{uu'}(t) = p(x,x',t;a_1,a_2)$.

The Kubo–Van Kampen operator cumulants of $\mathcal{G}$, e.g. $\langle \mathcal{G}(t)\mathcal{G}(s)\rangle_K$, are defined as in equations (2.22)–(2.23). As we will see in §3, the two-point PDF of the velocity field can be used to calculate important quantities such as the turbulent energy and indicator functions to stochastic shock clustering.

3. Stochastic simulations

The numerical simulation of the stochastic Burgers problem equation (2.1) has recently attracted considerable attention [51,52]. One difficult challenge is an effective computation of the solution in the inviscid limit, in particular in the presence of random forcing terms and random initial conditions. In fact, this could generate random shock waves at random space–time locations (see appendix A for a detailed description of shock waves in probability space). In this paper, we tackle this problem by using the adaptive DG method we have recently developed in [34] (see appendix B).

Let us first show that the numerical viscosity of the scheme dominates the conditional average term in equation (2.8), for $\nu \to 0$[5]. Such a term can be accurately computed by Monte Carlo simulation, i.e. by sampling a sufficiently large number of solutions to equation (2.1), and then averaging $u_{xx} = \partial^2 u/\partial x^2$, conditioned to $u(x,t;\omega) = a$ for arbitrary a. The results are shown in figure 2 for random flows solving equation (2.1) with initial condition

$$u_0(x;\eta) = \sin(x) + \eta(\omega) \tag{3.1}$$

and no random forcing. Here, η is a Gaussian random variable with mean 0 and variance 1/4. It is seen that the norm of conditional average term in equation (2.8) becomes smaller and smaller as ν goes to 0. In other words, at *finite numerical resolution* the solution to the PDF equation corresponding to the inviscid Burgers equation provides a very good approximation to the PDF of the inviscid limit of the solution to (2.1) after the shock occurrence, i.e. at $t = 1$ in the present example. To this end, we verify this by comparing the solutions computed by the joint PDF equation (2.8) with $\nu = 0$ to an accurate[6] MC solution to equation (2.1). In particular, we consider a prototype space-independent forcing term

$$f(x,t;\omega) = \xi(\omega)\sin(t), \tag{3.2}$$

where $\xi(\omega)$ and $\eta(\omega)$ are independent zero-mean Gaussian random variables with standard deviation $\pi/10$ and 1, respectively. In this hypothesis, the joint PDF of u_0 and ξ is

$$p(0) = \frac{5}{\pi^2}\exp\left[-\frac{(a-\sin(x))^2}{2}\right]\exp\left[-50\frac{b^2}{\pi^2}\right].$$

We set the amplitude of the random forcing term in equations (2.8) and (2.1) to $\sigma = 1$. The joint PDF equation (2.8) is solved by using the DG method with 50 elements of order $p = 4$ and 15th degree Hermite polynomials for the excitation space. Time-stepping is based on the fourth-order Runge–Kutta scheme with $\Delta t = 2 \times 10^{-4}$. In figure 3, we plot the results of our simulations, which show that the joint PDF solution coincides with the MC approach. Thus, in what follows we set $\nu = 0$ in all kinetic equations we obtained in §2. Note that the shock wave at $t = 1$ arising from the system does not arise in the response PDF shown in figure 3. Instead, such PDF solution looks rather smooth. As we will see in the next subsection, however, smooth multi-modal PDFs can generate flow realizations with discontinuities, i.e. shocks.

[5]All approaches and methodologies dealing with the numerical solution to the inviscid Burgers equation add an artificial (numerical) diffusion term which can be made arbitrarily small in some limiting process, e.g. by leveraging on *hp*-convergence. This means that we always have numerical non-uniqueness when computing the solution to the inviscid Burgers equation.

[6]Each solution sample is obtained by our adaptive DG method with a spatial discretization based on $N = 128$ finite elements of order $p = 8$ in $[0, 2\pi]$.

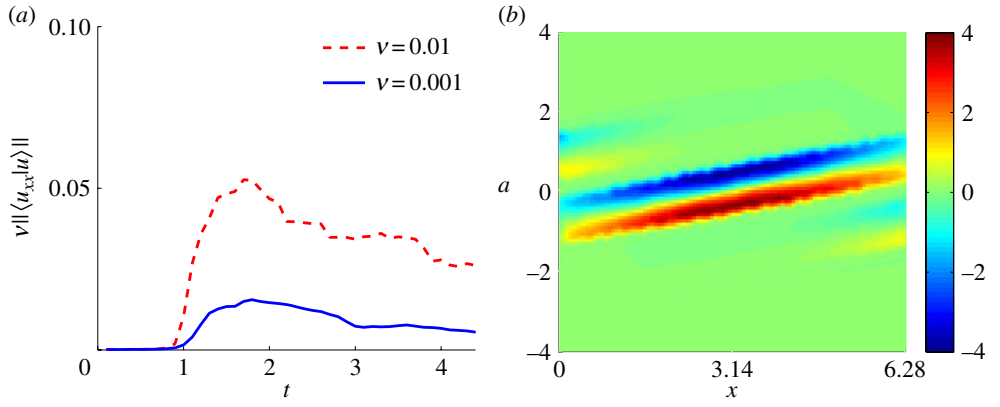

Figure 2. Numerical viscosity dominates the inviscid limit in the stochastic Burgers equation. In (*a*), we show a comparison of the L_2 norm of the conditional average $\langle u_{xx}|u\rangle$ for $\nu = 10^{-2}$ and $\nu = 10^{-3}$ versus time. At time $t = 1$, the inviscid limit of the solution to the Burgers equation subject to the random initial condition (3.1) generates an ensemble of shock waves. Figure (*b*) shows the contour values of $\langle u_{xx}|u\rangle$ for $\nu = 10^{-2}$ at time $t = 4$. Note that the minimum and the maximum values are located, respectively, near the peaks and the dips of the ensemble of shocks. (Online version in colour.)

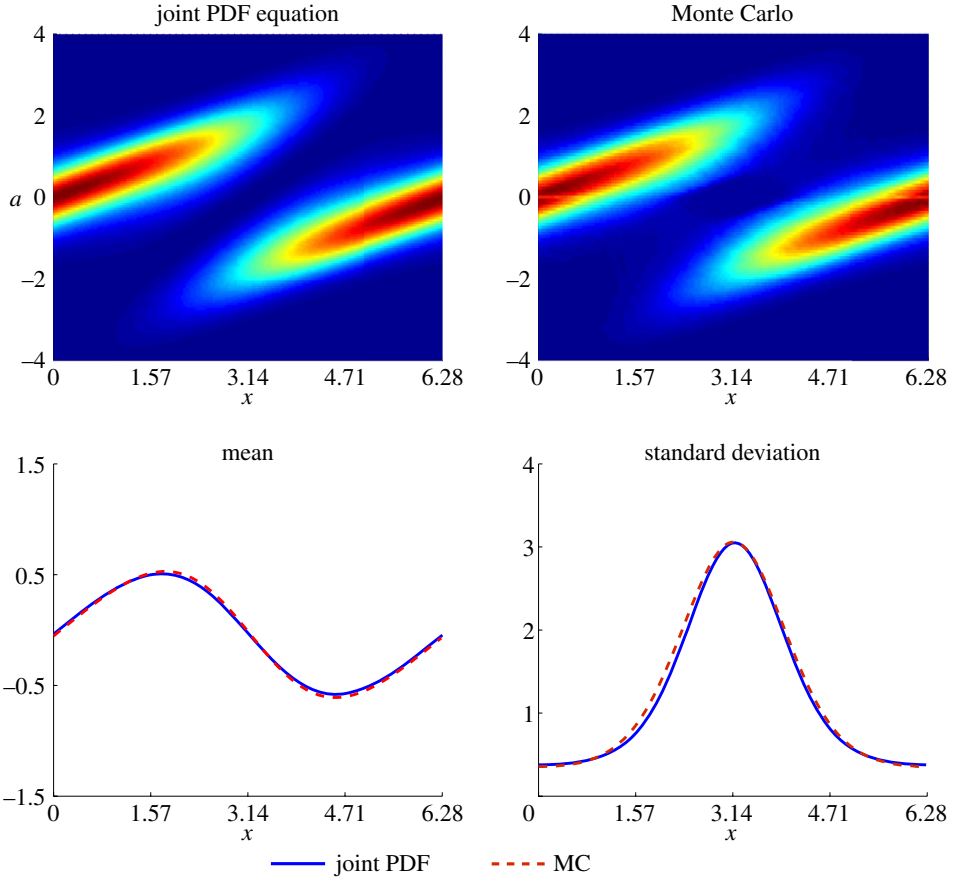

Figure 3. PDF of the velocity field: validation of the joint PDF equation. Shown is a comparison between the marginalized solution to equation (2.8) at $t = 1$ and a kernel density estimation [53] of the PDF of the velocity based on 50 000 MC samples. We also compare the mean and the standard deviation at $t = 1$ as computed from the PDF and the MC approaches. (Online version in colour.)

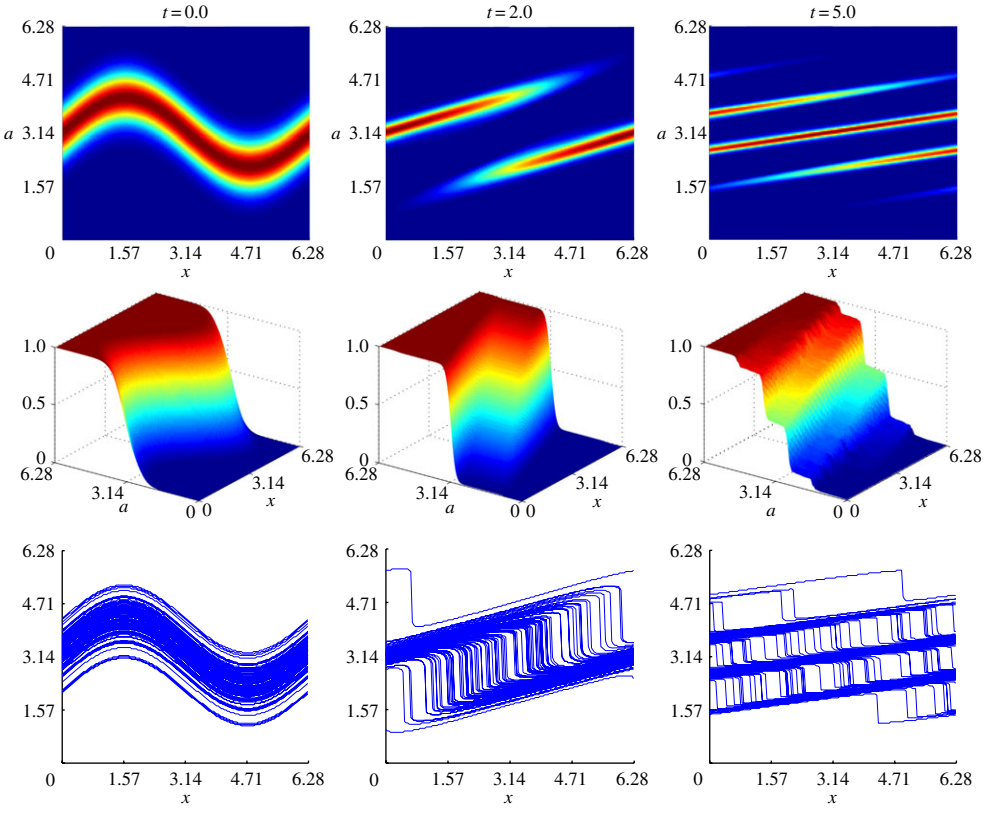

Figure 4. Shock realizations of the velocity field (third row) generated by smooth multi-modal PDFs (first row). The second row shows the cumulative density function of the PDFs of the first row. (Online version in colour.)

(a) High-dimensional random initial conditions

In this section, we present numerical results for various types of spatially correlated, high-dimensional random initial conditions. First of all, we show that a smooth multi-modal PDF can generate shock realizations. This is done in figure 4, where we consider the one-point PDF of the velocity field in the inviscid limit for initial conditions in equation (3.1). In contrast to the previous example where η was set to be zero mean, here we consider a Gaussian η with mean π and standard deviation $\pi/10$. The non-vanishing mean induces stirring of the PDF along the x-direction, yielding multi-modal patterns after short time. The corresponding cumulative distribution function (CDF) is defined as

$$C_u(t,x,a) \stackrel{\text{def}}{=} \int_{-\infty}^{a} p_u(t,x,a')\,\mathrm{d}a', \tag{3.3}$$

and it is plotted in the second row of figure 4. In the third row, we provide samples of the velocity field obtained from the CDF shown in the second row. It is seen that shock patterns can be generated from CDFs resembling a step function. In other words, the *location* and the *steepness* of the peaks in the one-point PDF can determine shock waves in the physical space.

However, as we point out in appendix A, the statistical information encoded in the one-point PDF is not sufficient to completely characterize the structure of shocks in space and time. Indeed, it is possible to manufacture a random initial condition problem for the inviscid Burgers equation having a significantly different shock structure in the physical space, but exactly the same one-point PDF dynamics. To this end, simply consider a set of i.i.d. normal random variables $\{\eta_k\}$, and

the Gaussian initial condition

$$u_0(x;\omega) = \frac{1}{\sqrt{m}} \sum_{k=1}^{m} [\eta_{2k}(\omega)\sin(kx) + \eta_{2k-1}(\omega)\cos(kx)], \tag{3.4}$$

whose one-point PDF is Gaussian with mean 0 and variance 1 at all spatial points x, disregarding m. For large values of m, we have very rough initial conditions developing shock discontinuities very early in time, while for small values of m we have smoother initial conditions developing shocks at later times. However, the one-point PDF dynamics predicted by equation (2.8) for $f = 0$ and $\nu \to 0$ is exactly the same. In other words, the one-point PDF does not encode enough statistical information to characterize shock dynamics and clustering. However, it allows us to compute all single-point statistical moments of the velocity field, as well as rare events (tails of the PDF).

(b) High-dimensional random forcing

The numerical simulation of the joint PDF equation (2.9) in the presence of a high-dimensional random forcing is a very challenging problem, as it involves the representation of a scalar field (the joint PDF) in a high-dimensional parametric space. For a moderate number of dimensions, effective approaches are multi-element and sparse adaptive probabilistic collocation [22,23,34]. On the other hand, the MZ projection operator formalism we developed in previous sections allows us to formally integrate out all the phase variables associated with the random forcing (i.e. the variables $\boldsymbol{b}$), yielding *low-dimensional* PDF equations in equation (2.21).

Let us first consider a zero-mean homogeneous (in space) Gaussian random process with exponential covariance function

$$\langle f(t;\boldsymbol{b}) f(s;\boldsymbol{b})\rangle_{\boldsymbol{b}} = \frac{1}{\tau}\exp\left[-\frac{|t-s|}{\tau}\right], \quad t,s \in [0,T],$$

where τ is the correlation time. Specifically, we choose $T = 5$ and $\tau = 0.01$, i.e. a nearly white-in-time Gaussian random process. The Karhunen–Loève (KL) expansion of such weakly correlated random forcing requires at least 57 random variables to achieve less than 5% error in the eigenspectrum. We first compute a benchmark PDF solution by solving equation (2.9) using sparse grid collocation of level 2 [54]. This entails sampling equation (2.9) at 6841 sparse grid points and then integrate the joint PDF $p(t)$ with respect to $\boldsymbol{b}$ in a 57-dimensional space by using appropriate quadrature rules. This benchmark solution is used to determine the accuracy of various truncations to the MZ-PDF equation (2.21), i.e. equation (2.28). This is done in figure 5, where we compare the one-point PDF of the velocity field at $x = \pi$ obtained by the first- and second-order approximations to equation (2.28). In the first-order approximation, we basically neglect all the terms of order σ^2 or higher. We see that when σ is small, e.g. $\sigma = 0.01$, both the first- and second-order approximations are in good agreement with the benchmark PDF solution up to $t = 5$. However, as σ becomes larger, the small-noise approximation based on the first- and second-order truncations slightly diverge from the MC benchmark solution. However, the computational cost of solving the second-order approximation to equation (2.28) in this case is less than 2% the cost of solving the exact equation (2.9). Therefore, the MZ-PDF framework provides a computationally efficient way to determine the one-point statistics of the velocity field.

(c) Burgers turbulence and the stochastic shock clustering

Let us go back to the flow example discussed in the Introduction, showing a realization of shock clustering and shock displacement induced by weak space–time additive forcing (see figure 1). The forcing term considered there was a sample of the space–time Gaussian random field

$$f(x,t;\boldsymbol{\xi}) = 1 + \sum_{k=1}^{5} [(-1)^k(\xi_{2k-1}\sin(2kx) + \xi_{2k}\cos(3kx))\,\mathrm{e}^{-\sin(2kt)}], \tag{3.5}$$

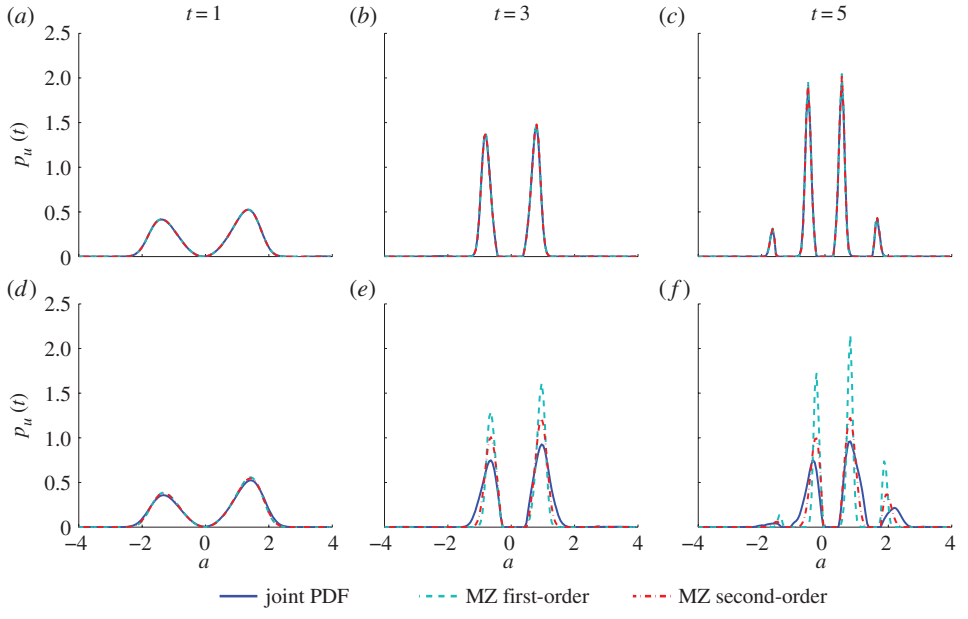

Figure 5. Randomly forced Burgers equation. One-point PDF of the velocity field at $x = \pi$ for exponentially correlated, homogeneous (in space) random forcing processes with correlation time $\tau = 0.01$ and amplitude $\sigma = 0.01$ (*a–c*) and $\sigma = 0.1$ (*d–f*). Shown are results obtained from the joint PDF equation (2.9), and two different truncations of the MZ-PDF equation (2.28). (Online version in colour.)

where ξ_k are jointly normal (independent) random variables, while the initial condition is an exponentially correlated random field represented in terms of a KL series expansion [55,56] in the form:

$$u_0(x;\omega) = a_0(\eta_0 + \sin(x)) + \sum_{k=1}^{m} \sqrt{\lambda_k}\eta_k \Psi_k(x), \tag{3.6}$$

where η_k are independent normal random variables, and λ_k and Ψ_k are, respectively, eigenvalues and eigenfunctions of the exponential covariance function

$$C(x,y) = \frac{1}{l_c}\exp\left(-\frac{|x-y|}{l_c}\right). \tag{3.7}$$

The quantity l_c denotes the spatial correlation length [57,58] of the random initial velocity (3.6). In figure 6, we show the time snapshots of the one-PDF of the velocity field obtained from the second-order approximation to the MZ equation (2.21). Specifically, we consider an initial condition in the form (3.6) with $l_c = 0.01$, and the forcing term (3.5) with amplitude $\sigma = 0.05$.

As pointed out in appendix A, the one-point PDF of the solution field does not tell us anything about the structure of shocks in space and time, thus about shock clustering. Therefore, if we are interested in studying this phenomenon, we should resort to other functionals of the velocity field, in particular on asymptotic properties. In Burgers turbulence, these can be grouped into two main classes: (i) *universal properties* that are independent of initial or boundary conditions, and (ii) properties that depend heavily on such conditions. For instance, the k^{-2} slope in the inertial range of the energy spectrum is a universal property while the time-evolution of the kinetic energy per unit length is not [6,59]. Many universal properties can be defined in terms of the two-point correlation function, e.g.

$$\mathcal{J}(t) \overset{\text{def}}{=} \frac{1}{2\pi}\int_0^{2\pi}\int_{\mathbb{R}} \langle u(x,t)u(x+r,t)\rangle \,\mathrm{d}r\,\mathrm{d}x, \tag{3.8}$$

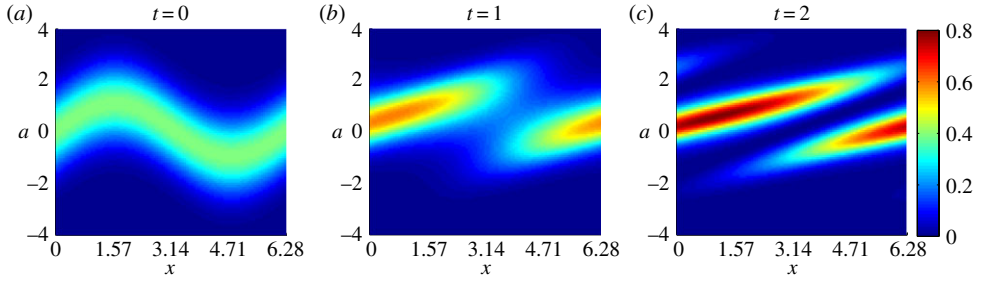

Figure 6. (*a–c*) Burgers turbulence. Time snapshots of the one-point PDF obtained from the second-order approximation to the MZ equation (2.21). We consider a rough initial condition in the form (3.6) with $l_c = 0.01$, and the forcing term (3.5) with amplitude $\sigma = 0.05$. (Online version in colour.)

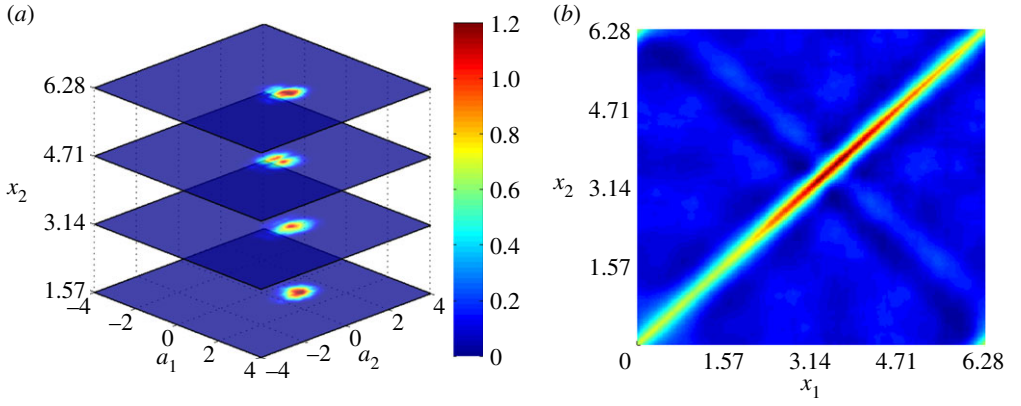

Figure 7. Slices of two-point PDF of the velocity field at $t = 1$ (*a*) and velocity correlation function (*b*). Specifically, in (*a*) we plot the two-point PDF field at $x_1 = \pi/4$ and four other points $x_2 = \{\pi/2, \pi, 3\pi/2, 2\pi\}$. (Online version in colour.)

and the power spectral density

$$\tilde{E}(k,t) \overset{\text{def}}{=} \frac{1}{2\pi}\int_0^{2\pi} E(x,k,t)\,\mathrm{d}x, \tag{3.9}$$

where

$$E(x,k,t) = \frac{1}{2\pi}\int_{\mathbb{R}} \cos(kr)[\langle u(x,t)u(x+r,t)\rangle - \langle u(x,t)\rangle\langle u(x+r,t)\rangle]\,\mathrm{d}r. \tag{3.10}$$

$\mathcal{J}(t)$ is known to be invariant in time [60]. Another interesting quantity which is ultimately related to *stochastic shock clustering* [3,61] is the turbulent energy per unit length

$$\mathcal{E}(t) \overset{\text{def}}{=} \frac{1}{2\pi}\int_0^{2\pi} \hat{E}(x,t)\,\mathrm{d}x \quad \text{where } \hat{E}(x,t) \overset{\text{def}}{=} \int_0^{\infty} E(x,k,t)\,\mathrm{d}k. \tag{3.11}$$

The two-point correlation function appearing in equations (3.8), (3.10) and (3.11) can be determined by integrating the solution to the two-point MZ-PDF equation (2.33) as (see figure 7)

$$\langle u(x,t)u(x+r,t)\rangle = \int_{-\infty}^{\infty}\int_{-\infty}^{\infty} a_1 a_2 p(x,x+r,t;a_1,a_2)\,\mathrm{d}a_1\,\mathrm{d}a_2. \tag{3.12}$$

In figure 8, we plot the power spectral density (3.9) and the normalized turbulent energy per unit length (3.11) for random initial conditions (3.6) with different correlation lengths l_c and random forcing terms (3.5) of different amplitude σ. It is seen that for $\sigma = 0$ the slope of the power spectral density in the inertial range is k^{-2}, independently of l_c. This is in agreement with

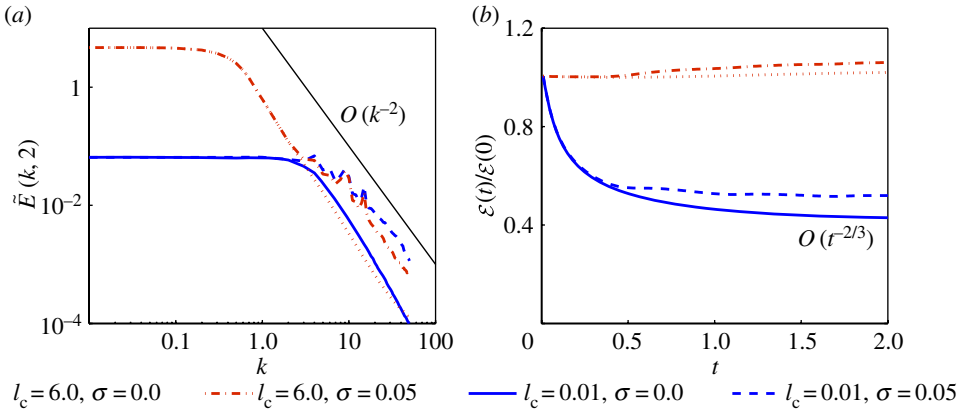

Figure 8. Stochastic Burgers turbulence simulations. Shown is the k^{-2} decay of the power spectral density in the inertial range (*a*). This property does not depend on the correlation length l_c of the initial condition, i.e. it is a universal property. On the contrary, the dynamics of the normalized turbulent energy per unit length (*b*) heavily depends on the specific choice of initial conditions. In particular, for rough initial conditions (i.e. those with small correlation length l_c) we observe a rapid decay of the turbulent energy due to shock clustering. After that, the train of triangular shocks settles down to a similarity state where the turbulent energy decays approximately as $t^{-2/3}$, in agreement with classical results of dimensional analysis. Random forcing terms of small amplitude σ inject additional energy into the system. As a consequence, we observe a perturbation in the energy spectrum (*a*), and an increase in the turbulent energy per unit length (*b*). (Online version in colour.)

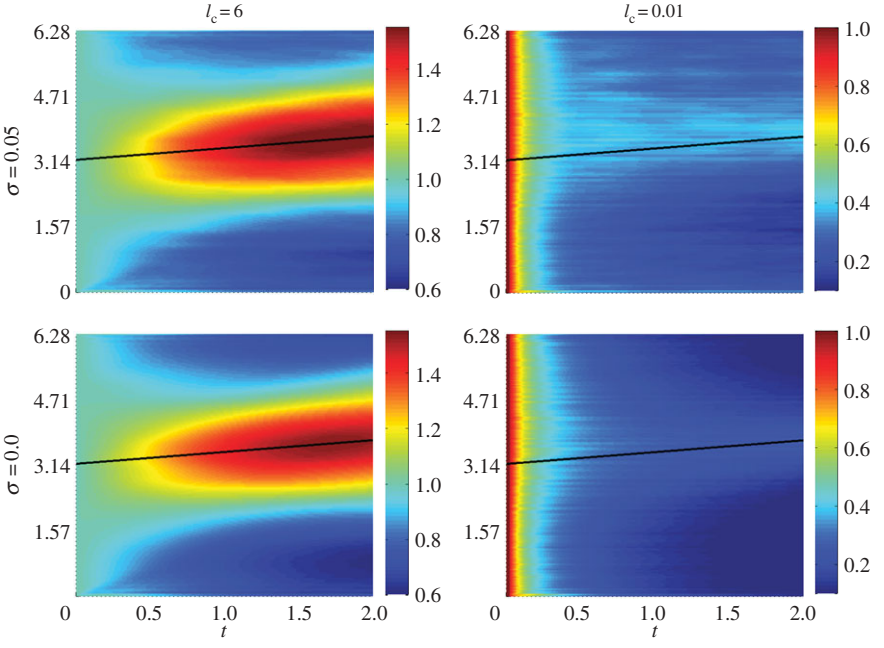

Figure 9. Space–time portraits of the normalized turbulent energy in Burgers turbulence. Specifically, we plot $\mathcal{E}(x,t)/\mathcal{E}(x,0)$ (3.11) for random initial conditions (3.6) with different correlation lengths l_c and random forcing terms (3.5) of different amplitudes σ. It is seen that the normalized turbulent energy is an indicator function of stochastic shock clustering for rough random initial conditions. In particular, the initial rapid decay of the turbulent energy observed for $l_c = 0.01$ corresponds to the transient dynamics in which the velocity field is regularized by shock clustering (see sample solutions in figure 1) before settling down to the similarity state. The black line in each plot indicates the shock front associated with the $\sin(x)$ term in (3.6). Such contribution is responsible for the increase in the normalized turbulent energy, in particular for initial conditions with large correlation lengths. (Online version in colour.)

classical results on Burgers turbulence. We also observe a perturbation in the energy spectrum due to the energy injected in the system through the random forcing term. This slightly increases the turbulent energy per unit length, relatively to the case where there is no forcing. Note that rough random initial conditions, i.e. those with correlation length $\ell = 0.01$, are associated with an initial rapid decay of the normalized turbulent energy due to shock clustering (see also figure 9). Later on, the train of triangular shocks settles down to a similarity state where the turbulent energy decays approximately as $t^{-2/3}$, in agreement with classical results of Tokunaga [62] and Kida [6]. In figure 9, we plot the space–time portraits of the normalized turbulent energy $\hat{E}(x,t)/\hat{E}(x,0)$, where $\hat{E}(x,t)$ is defined in equation (3.11). It is seen that the turbulent energy undergoes a rapid decay for initial conditions with short correlation length, i.e. for $l_c = 0.01$. Such rapid decay corresponds to the transient dynamics in which the velocity field is regularized by shock clustering (see sample solutions in figure 1) before settling down to the similarity state. The black line in each plot indicates the shock front associated with the $\sin(x)$ term in (3.6). Such contribution is responsible for the increase in the normalized turbulent energy, in particular for initial conditions with large correlation lengths.

4. Summary

In this paper, we studied the statistical properties of random shock waves governed by the stochastic Burgers equation subject to high-dimensional random initial conditions and additive random forcing terms. We revisited this fundamental problem of classical fluid mechanics and provided new insights into the analysis of the underlying nonlinear processes. Specifically, by using the MZ formulation of irreversible statistical mechanics, we derived reduced-order PDF equations for the one- and the two-point PDFs of the velocity field in the inviscid limit and computed their numerical solution by using our recently developed adaptive (shock-capturing) DG method. We demonstrated that the regularization effect induced in the PDF dynamics by finite numerical resolution (numerical viscosity of the scheme) dominates the diffusion term in the inviscid limit, but does not affect the statistical properties of the solution significantly. We also addressed the question of how random shock waves in space–time manifest themselves in probability space. By using a relatively simple problem, we have shown that there are two main sources of shocks in the one-point PDF of a random field: (i) discontinuities of the random field in space and time and (ii) compactness of the range of the random variables underlying the random field. At the same time, by using simple arguments we proved that information on shock dynamics and clustering is not encoded in the one-point PDF. This is due to the large number of statistical symmetries satisfied by the one-point PDF, the simplest one being sample-relabelling symmetry. However, by using the two-point PDF of the velocity field, whose exact dynamics is governed by an MZ-type equation, we can compute important quantities, such as the turbulent energy, which is ultimately related to shock dynamics and clustering. In future work, we will compute energy and probability fluxes at various scales by using the two-point PDF equation, which is of fundamental importance, e.g. in the inverse cascade of vorticity arising in two-dimensional turbulence [63,64]. In addition, the approach presented in this paper can be extended to more general systems of randomly perturbed scalar conservation laws and nonlinear PDEs. This is useful to many disciplines and it may lead to new insights into high-dimensional stochastic dynamics and also the development of more efficient computational algorithms.

Acknowledgements. This work was supported by OSD-MURI grant FA9550-09-1-0613, by DOE grant DE-SC0009247 and NSF/DMS-1216437 grant.

Appendix A. Shock waves in probability space

A fundamental question related to the existence of random shock waves generated by stochastic conservation laws is the following: *Can random shocks in space–time induce shocks in probability space?* In this section, we address this question by using a simple toy problem, and subsequently examine what happens in the more general case of stochastic Burgers equation. Let us first show that the

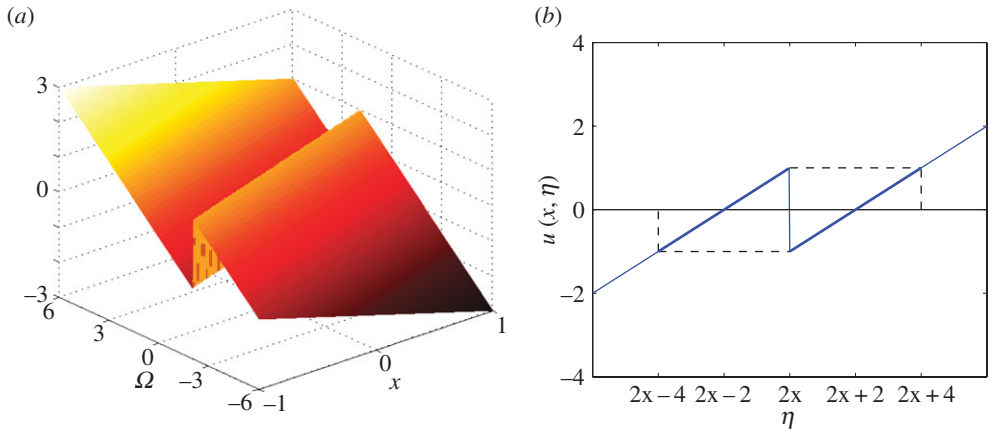

Figure 10. Random field (A 1) (*a*) and its level sets at fixed x (*b*). The field has a line discontinuity of magnitude 2 with fixed peaks and dips at ± 1, respectively. (Online version in colour.)

PDF of a discontinuous random field can indeed be discontinuous. In particular, let us consider

$$u(x;\eta) = \begin{cases} -x + \frac{1}{2}\eta - 1, & x \le \frac{\eta}{2}, \\ -x + \frac{1}{2}\eta + 1, & x \ge \frac{\eta}{2}, \end{cases} \tag{A 1}$$

where η is a random variable. As shown in figure 10, the shock is located at $x = \eta/2$, i.e. at a random location whose distribution is related to that of η. The PDF of $u(x;\omega)$ can be computed by using the classical mapping approach [65], given the PDF of η. Specifically, let us first assume that η is Gaussian, i.e.

$$p_\eta(a) = \sqrt{\frac{2}{\pi}}\, \mathrm{e}^{-2a^2}.$$

This yields

$$p_u(a,x) = \left[2\sqrt{\frac{2}{\pi}}\, \mathrm{e}^{-8(a+x-1)^2}\right] \chi_{\{a \le 1\}} + \left[2\sqrt{\frac{2}{\pi}}\, \mathrm{e}^{-8(a+x+1)^2}\right] \chi_{\{a \ge -1\}}, \tag{A 2}$$

where χ_A is the *indicator function* of the set A. As shown in figure 11*a*, the PDF (A 2) exhibits two shocks at $a = -1$ and 1. Note that these coincide with the left and the right limits of the field (A 1) at the shock location. Similarly, if we assume that η is a uniform random variable in $[-6, 6]$, we obtain

$$p_u(a,x) = \frac{1}{6}\chi_{[-x-2,1]} + \frac{1}{6}\chi_{[-1,-x+2]}.$$

This PDF is plotted in figure 11*b*. We note that, in this case, the PDF exhibits shock discontinuities because of distinct values of the random field at the shock location, but also because the range of η is compact, i.e. $[-6, 6]$. Hence, discontinuities in the one-point PDF of a random field can be induced by two main factors:

(i) Random shocks in space and time;
(ii) Compactness of the range of the random variables describing the random field.

Going back to the question we addressed at the beginning of this section, it is now clear that random shocks in space and time *can* induce shocks in the one-point PDF of the random field. However, this is not always the case. In fact, we can also have situations where ensembles of fields with shocks yield smooth one-point PDFs. This suggests that information on shock clustering in physical space might not be encoded in the one-point PDF of the solution to the Burgers problem

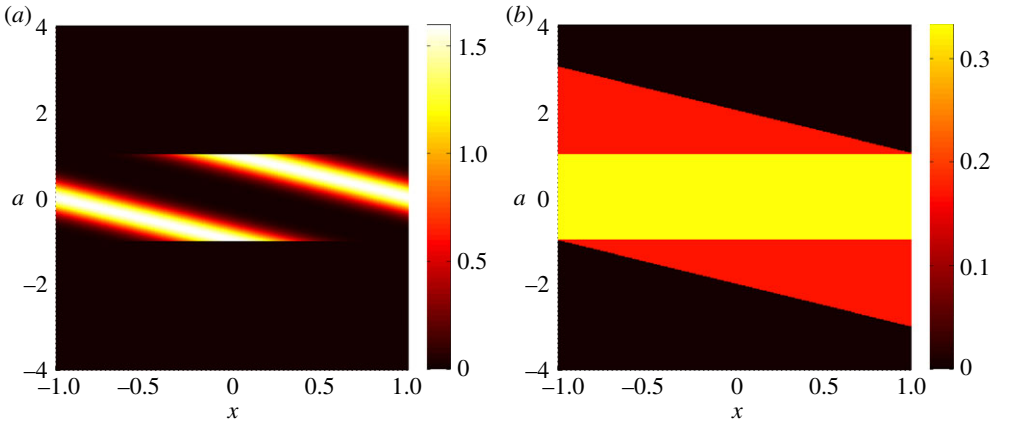

Figure 11. Shock waves in probability space. Shown is the one-point PDF of the discontinuous random field (A 1) in the case where η is Gaussian (*a*) or uniform (*b*) random variable. The shock wave in the PDF can be generated either by physical discontinuities in the random field or by the compactness of the range of the underlying random variables. (Online version in colour.)

(2.1). We addressed this important point in §3. Summarizing the main results of this section we can say that

— random fields with shocks can induce shocks in the one-point PDF;
— the one-point PDF of ensembles of fields with shocks can be smooth; and
— the one-point PDF of random fields does not provide any information about the structure of shocks in space and time.

In this paper, we studied the PDF dynamics of the solution to the inviscid stochastic Burgers problem (2.1). In particular, we focused on one- and two-point distributions associated with various types of random initial conditions and random forcing terms.

Appendix B. Discontinuous Galerkin method for kinetic equations

The variables appearing in the solution to the joint PDF equation (2.8) can be grouped into two main classes, i.e. those belonging to the response space and those belonging to the excitation space. The response space is a subset of $\mathbb{R}^2$ that includes the phase variable a and the coordinate x. On the other hand, the excitation space is a subset of $\mathbb{R}^m$ that includes the variables $\boldsymbol{b}$, which appear simply as parameters in (2.8). The response space can be discretized by using the DG method [34]. As is well known, the DG method has many good features of both finite volume and finite element methods, such as conservative property, flexibility in choosing the elements and *hp*-adaptivity [66,67]. In order to illustrate the application of the DG method to the kinetic equation (2.8), let us rewrite it as a hyperbolic conservation law, i.e.

$$\frac{\partial p(t)}{\partial t} = -\nabla \cdot \boldsymbol{F}[p(t)], \tag{B 1}$$

where

$$\nabla \stackrel{\text{def}}{=} \left(\frac{\partial}{\partial x}, \frac{\partial}{\partial a} \right) \quad \text{and} \quad \boldsymbol{F}[p] \stackrel{\text{def}}{=} \left\{ \int_{-\infty}^{a} p(t)\, \mathrm{d}a' + ap(t), \sigma f(x,t;\boldsymbol{b}) p(t) \right\} \tag{B 2}$$

are, respectively, the gradient operator and the flux. Next, we consider a spectral element discretization of the response space, i.e. the phase and physical space described by the variables a and x. Specifically, we select a bounded computational domain $\Omega \subseteq \mathbb{R}^n$, which is large enough

to include the support of the joint PDF $p(t)$. This allows us to set homogeneous conditions at the boundary of Ω. Let Ω_h be a triangulation of Ω, consisting of elements K_i ($i=1,\ldots,N_{\mathrm{el}}$), i.e.

$$\Omega = \bigcup_{i=1}^{N_{\mathrm{el}}} K_i, \quad K_i \in \Omega_h. \tag{B 3}$$

We look for a solution to (B 1) in the finite element space

$$\mathcal{V}_h \stackrel{\mathrm{def}}{=} \{v \in L_2(\Omega) : v|_{K_i} \in H^p(K_i)\ \forall\, K_i \in \Omega_h\}. \tag{B 4}$$

Here, $H^p(K_i)$ denotes the space of polynomials of degree at most p in n variables within the element K_i. Note that we are not imposing any continuity requirement for the solution between adjacent elements. The spectral-element solution to (B 1) can be written as

$$\hat{p}(x,a,\boldsymbol{b},t) = \sum_{i=1}^{N_{\mathrm{el}}} \hat{p}_i(x,a,\boldsymbol{b},t), \quad \hat{p}_i(x,a,\boldsymbol{b},t) \stackrel{\mathrm{def}}{=} \sum_{j=0}^{d} \alpha^j_{K_i}(t,\boldsymbol{b})\psi^j_{K_i}(x,a), \tag{B 5}$$

where d denotes the number of degrees of freedom within each element K_i, and $\psi^j_{K_i}(a) \in H^p(K_i)$ ($j=1,\ldots,d$) is the set of basis functions in the element K_i. We substitute (B 5) into (B 1) and impose that the residual is orthogonal to the finite element space $\mathcal{V}_h$. By using the simplified notation $\hat{p} = \hat{p}(x,a,\boldsymbol{b},t)$, this yields the following element-wise Galerkin formulation

$$\int_{K_i} q \frac{\partial \hat{p}}{\partial t}\,\mathrm{d}K_i = \int_{K_i} \nabla_a q \cdot \boldsymbol{F}[\hat{p}]\,\mathrm{d}K_i - \int_{\partial K_i} q\boldsymbol{F}[\hat{p}]\cdot \boldsymbol{n}_i\,\mathrm{d}S_i \quad \forall\, q \in H^p(K_i), \tag{B 6}$$

where $\boldsymbol{n}_i$ denotes the outward normal unit vector on the boundary ∂K_i. An important part of the solution process is the evaluation of the multidimensional flux $\boldsymbol{F}[\hat{p}]$ through the element boundary ∂K_i, i.e. the computation of the last integral in (B 6). Since we allowed discontinuous solutions across adjacent elements, the value of $\boldsymbol{F}[\hat{p}]$ is not unique on ∂K_i. Therefore, we replace $\boldsymbol{F}[\hat{p}]$ with the *numerical flux* $\tilde{\boldsymbol{F}}[\hat{p}_-,\hat{p}_+]$, representing the information transferred through the boundary of adjacent elements. The quantities $\hat{p}_-$ and $\hat{p}_+$ here represent, respectively, the finite element solution within the element K_i and the solution within the adjacent ones. Among various schemes to compute the numerical flux $\tilde{\boldsymbol{F}}[\hat{p}_-,\hat{p}_+]$, we consider here the Godunov's scheme [66], which has good conservative property and works well for discontinuous solutions. Such a scheme can be explicitly written as

$$\tilde{F}_j[\hat{p}_-,\hat{p}_+] = \begin{cases} \min\limits_{p_m \le p \le p_M} F_j[\hat{p}], & \bar{a} \ge 0, \\ \max\limits_{p_m \le p \le p_M} F_j[\hat{p}], & \bar{a} < 0, \end{cases} \quad \bar{a} = \frac{F_j[\hat{p}_+] - F_j[\hat{p}_-]}{\hat{p}_+ - \hat{p}_-},$$

where $\tilde{F}_j$ ($j=1,2$) denotes the component of the numerical flux along the direction a and x, $p_m = \min(p_-,p_+)$, and $p_M = \max(p_-,p_+)$.

References

1. Hopf E. 1950 The partial differential equation $u_t + uu_x = u_{xx}$. *Commun. Pure Appl. Math.* **3**, 201–230. (doi:10.1002/cpa.3160030302)
2. Cole JD. 1951 On a quasi-linear parabolic equations occurring in aerodynamics. *Quart. Appl. Math* **9**, 225–236.
3. Menon G, Srinivasan R. 2010 Kinetic theory and Lax equations for shock clustering and Burgers turbulence. *J. Stat. Phys.* **140**, 1195–1223. (doi:10.1007/s10955-010-0028-3)
4. Gurbatov SN, Simdyankin SI, Aurell E, Frisch U, Tòth T. 1997 On the decay of Burgers turbulence. *J. Fluid. Mech.* **344**, 339–374. (doi:10.1017/S0022112097006241)
5. Gotoh T, Kraichnan RH. 1993 Statistics of decaying Burgers turbulence. *Phys. Fluids* **5**, 445–457. (doi:10.1063/1.858868)
6. Kida S. 1979 Asymptotic properties of Burgers turbulence. *J. Fluid. Mech.* **93**, 337–377. (doi:10.1017/S0022112079001932)

7. Avellaneda M, Weinan E. 1995 Statistical properties of shocks in Burgers turbulence. *Commun. Math. Phys.* **172**, 13–38. (doi:10.1007/BF02104509)
8. Avellaneda M. 1995 Statistical properties of shocks in Burgers turbulence, II: tail probabilities for velocities, shock-strengths and rarefaction intervals. *Commun. Math. Phys.* **169**, 45–59. (doi:10.1007/BF02101596)
9. Frachebourg L, Martin PA. 2000 Exact statistical properties of the Burgers equation. *J. Fluid. Mech.* **417**, 323–349. (doi:10.1017/S0022112000001142)
10. She ZS, Aurell E, Frisch U. 1992 The inviscid Burgers equation with initial data of Brownian type. *Commun. Math. Phys.* **148**, 623–641. (doi:10.1007/BF02096551)
11. Valageas P. 2009 Some statistical properties of the Burgers equation with white-noise initial velocity. *J. Stat. Phys.* **137**, 729–764. (doi:10.1007/s10955-009-9809-y)
12. Bertini L, Cancrini N, Jona-Lasinio G. 1994 The stochastic Burgers equation. *Commun. Math. Phys.* **165**, 211–232. (doi:10.1007/BF02099769)
13. Sinai YG. 1992 Statistics of shocks in solutions of inviscid Burgers equation. *Commun. Math. Phys.* **148**, 601–621. (doi:10.1007/BF02096550)
14. Valageas P. 2009 Statistical properties of the Burgers equation with Brownian initial velocity. *J. Stat. Phys.* **134**, 589–640. (doi:10.1007/s10955-009-9685-5)
15. Garnier J, Papanicolau G, Yang T-W. 2013 Anomalous shock displacement probabilities for a perturbed scalar conservation law. *Multiscale Model. Simul.* **11**, 1000. (doi:10.1137/120883864)
16. Polyakov AM. 1995 Turbulence without pressure. *Phys. Rev. E* **52**, 6183–6188. (doi:10.1103/PhysRevE.52.6183)
17. Eule S, Friedrich R. 2006 A note on the forced Burgers equation. *Phys. Lett. A* **351**, 238–241. (doi:10.1016/j.physleta.2005.11.019)
18. Weinan E, Khanin K, Mazel A, Sinai Y. 2000 Invariant measures for Burgers equation with stochastic forcing. *Ann. Math.* **151**, 877–960. (doi:10.2307/121126)
19. Ghanem RG, Spanos PD. 1998 *Stochastic finite elements: a spectral approach*. Berlin, Germany: Springer.
20. Xiu D, Karniadakis GE. 2002 The Wiener–Askey polynomial chaos for stochastic differential equations. *SIAM J. Sci. Comput.* **24**, 619–644. (doi:10.1137/S1064827501387826)
21. Wan X, Karniadakis GE. 2006 Multi-element generalized polynomial chaos for arbitrary probability measures. *SIAM J. Sci. Comput.* **28**, 901–928. (doi:10.1137/050627630)
22. Doostan A, Owhadi H. 2011 A non-adapted sparse approximation of PDEs with stochastic inputs. *J. Comput. Phys.* **230**, 3015–3034. (doi:10.1016/j.jcp.2011.01.002)
23. Foo J, Karniadakis GE. 2010 Multi-element probabilistic collocation method in high dimensions. *J. Comput. Phys.* **229**, 1536–1557. (doi:10.1016/j.jcp.2009.10.043)
24. Li G, Wang S-W, Rabitz H, Wang S, Jaffé P. 2002 Global uncertainty assessments by high dimensional model representations (HDMR). *Chem. Eng. Sci.* **57**, 4445–4460. (doi:10.1016/S0009-2509(02)00417-7)
25. Venturi D. 2011 A fully symmetric nonlinear biorthogonal decomposition theory for random fields. *Physica D* **240**, 415–425. (doi:10.1016/j.physd.2010.10.005)
26. Sapsis TP, Lermusiaux PFJ. 2009 Dynamically orthogonal field equations for continuous stochastic dynamical systems. *Physica D* **238**, 2347–2360. (doi:10.1016/j.physd.2009.09.017)
27. Doostan A, Validib A, Iaccarino G. 2013 Non-intrusive low-rank separated approximation of high-dimensional stochastic models. *Comput. Methods Appl. Mech. Eng.* **263**, 42–55. (doi:10.1016/j.cma.2013.04.003)
28. Nouy A. 2010 Proper generalized decompositions and separated representations for the numerical solution of high dimensional stochastic problems. *Arch. Comput. Methods Appl. Mech. Eng.* **17**, 403–434. (doi:10.1007/s11831-010-9054-1)
29. Venturi D, Karniadakis GE. 2013 Convolutionless Nakajima–Zwanzig equations for stochastic analysis in nonlinear dynamical systems. *Proc. R. Soc. A* **470**, 20130754. (doi:10.1098/rspa.2013.0754)
30. Zwanzig R. 1961 Memory effects in irreversible thermodynamics. *Phys. Rev.* **124**, 983–992. (doi:10.1103/PhysRev.124.983)
31. Breuer H-P, Kappler B, Petruccione F. 2001 The time-convolutionless projection operator technique in the quantum theory of dissipation and decoherence. *Ann. Phys.* **291**, 36–70. (doi:10.1006/aphy.2001.6152)
32. Chaturvedi S, Shibata F. 1979 Time-convolutionless projection operator formalism for elimination of fast variables. Applications to Brownian motion. *Z. Phys. B* **35**, 297–308. (doi:10.1007/BF01319852)

33. Faetti S, Fronzoni L, Grigolini P, Mannella R. 1988 The projection operator approach to the Fokker–Planck equation. I. Colored Gaussian noise. *J. Stat. Phys.* **52**, 951–978. (doi:10.1007/BF01019735)
34. Cho H, Venturi D, Karniadakis G. 2013 Adaptive discontinuous Galerkin method for response-excitation PDF equations. *SIAM J. Sci. Comput.* **35**, B890–B911. (doi:10.1137/12088896X)
35. Prato GD, Zabczyk J. 1992 *Stochastic equations in infinite dimensions*. Cambridge, UK: Cambridge University Press.
36. Prato GD, Debussche A, Temam R. 1994 Stochastic Burgers equation. *Nonlinear Differential Equations Appl.* **1**, 389–402. (doi:10.1007/BF01194987)
37. Venturi D, Karniadakis GE. 2012 New evolution equations for the joint response-excitation probability density function of stochastic solutions to first-order nonlinear PDEs. *J. Comput. Phys.* **231**, 7450–7474. (doi:10.1016/j.jcp.2012.07.013)
38. Venturi D, Tartakovsky DM, Tartakovsky AM, Karniadakis GE. 2013 Exact PDF equations and closure approximations for advective–reactive transport. *J. Comput. Phys.* **243**, 323–343. (doi:10.1016/j.jcp.2013.03.001)
39. Khuri AI. 2004 Applications of Dirac's delta function in statistics. *Int. J. Math. Educ. Sci. Technol.* **35**, 185–195. (doi:10.1080/00207390310001638313)
40. Pope SB. 1994 Lagrangian PDF methods for turbulent flows. *Annu. Rev. Fluid Mech.* **26**, 23–63. (doi:10.1146/annurev.fl.26.010194.000323)
41. Weinan E, Eijnden EV. 2000 Statistical theory for the stochastic Burgers equation in the inviscid limit. *Commun. Pure Appl. Math.* **53**, 852–901. (doi:10.1002/(SICI)1097-0312(200007)53:7<852::AID-CPA3>3.0.CO;2-5)
42. Grinstein FF, Margolin LG, Rider WJ. 2011. *Implicit large eddy simulation: computing turbulent fluid dynamics*. Cambridge, UK: Cambridge University Press.
43. Van Kampen NG. 1974 A cumulant expansion for stochastic linear differential equations. II. *Physica* **74**, 239–247. (doi:10.1016/0031-8914(74)90122-0)
44. Van Kampen NG. 2007. *Stochastic processes in physics and chemistry*, 3rd edn. Amsterdam, The Netherlands: North-Holland.
45. Al-Mohy AH, Higham NJ. 2011 Computing the action of the matrix exponential with an application to exponential integrators. *SIAM J. Sci. Comput.* **33**, 488–511. (doi:10.1137/100788860)
46. Moler C, Loan CV. 2003 Nineteen dubious ways to compute the exponential of a matrix, twenty-five years later. *SIAM Rev.* **45**, 3–49. (doi:10.1137/S00361445024180)
47. Edwards WS, Tuckerman LS, Friesner RA, Sorensen DC. 1994 Krylov methods for the incompressible Navier–Stokes equations. *J. Comput. Phys.* **110**, 82–102. (doi:10.1006/jcph.1994.1007)
48. Tokman M, Loffeld J. 2010 Efficient design of exponential-Krylov integrators for large scale computing. *Procedia Comput. Sci.* **1**, 229–237. (doi:10.1016/j.procs.2010.04.026)
49. Kato T. 1995 *Perturbation theory for linear operators*, 4th edn. Berlin, Germany: Springer.
50. Engel K-J, Nagel R. 2000 *One-parameter semigroups for linear evolution equations*. Berlin, Germany: Springer.
51. Hairer M, Voss J. 2011 Approximation to the stochastic Burgers equation. *J. Nonlinear Sci.* **21**, 897–920. (doi:10.1007/s00332-011-9104-3)
52. Blömker D, Jentzen A. 2013 Galerkin approximations for the stochastic Burgers equation. *SIAM J. Numer. Anal.* **51**, 694–715. (doi:10.1137/110845756)
53. Botev ZI, Grotowski JF, Kroese DP. 2010 Kernel density estimation via diffusion. *Ann. Statist.* **38**, 2916–2957. (doi:10.1214/10-AOS799)
54. Nobile F, Tempone R, Webster C. 2008 A sparse grid stochastic collocation method for partial differential equations with random input data. *SIAM J. Numer. Anal.* **46**, 2309–2345. (doi:10.1137/060663660)
55. Cho H, Venturi D, Karniadakis GE. 2013 Karhunen–Loéve expansion for multi-correlated stochastic processes. *Probab. Eng. Mech.* **34**, 157–167. (doi:10.1016/j.probengmech.2013.09.004)
56. Jardak M, Su C-H, Karniadakis GE. 2002 Spectral polynomial chaos solutions of the stochastic advection equation. *J. Sci. Comput.* **17**, 319–338. (doi:10.1023/A:1015125304044)
57. Venturi D, Wan X, Karniadakis GE. 2008 Stochastic low-dimensional modelling of a random laminar wake past a circular cylinder. *J. Fluid Mech.* **606**, 339–367. (doi:10.1017/S0022112008001821)

58. Venturi D, Choi M, Karniadakis GE. 2012 Supercritical quasi-conduction states in stochastic Rayleigh–Bénard convection. *Int. J. Heat Mass Transfer* **55**, 3732–3743. (doi:10.1016/j.ijheatmasstransfer.2012.03.033)
59. Hosokawa I, Yamamoto K. 1970 Numerical study of the Burgers' model of turbulence based on the characteristic functional formalism. *Phys. Fluids* **13**, 1683–1692. (doi:10.1063/1.1693141)
60. Burgers JM. 1974 *The nonlinear diffusion equation*. Dordrecht, The Netherlands: Reidel.
61. Srinivasan R. 2012 An invariant in shock clustering and Burgers turbulence. *Nonlinearity* **25**, 781–789. (doi:10.1088/0951-7715/25/3/781)
62. Tokunaga H. 1983 A numerical study of the Burgers turbulence at extremely large Reynolds numbers. *J. Phys. Soc. Jpn.* **52**, 827–833. (doi:10.1143/JPSJ.52.827)
63. Friedrich R, Daitche A, Kamps O, Lülff J, Vobkuhle M, Wilczek M. 2012 The Lundgren–Monin–Novikov hierarchy: kinetic equations for turbulence. *C. R. Physique* **13**, 929–953. (doi:10.1016/j.crhy.2012.09.009)
64. Friedrich R, Vobkuhle M, Kamps O, Wilczek M. 2012 Two-point vorticity statistics in the inverse cascade of two-dimensional turbulence. *Phys. Fluid* **24**, 125101. (doi:10.1063/1.4767465)
65. Papoulis A. 1991 *Probability, random variables and stochastic processes*, 3rd edn. New York, NY: McGraw-Hill.
66. Cockburn B, Karniadakis GE, Shu C-W. 2000 *Discontinuous Galerkin methods*. Lecture Notes in Computational Science and Engineering, vol. 11. Berlin, Germany: Springer.
67. Cockburn B, Shu C-W. 2001 Runge–Kutta discontinuous Galerkin methods for convection dominated problems. *J. Sci. Comput.* **16**, 173–261. (doi:10.1023/A:1012873910884)